CAPACITANCE MEASUREMENTS

An Analysis of the Phase Detector Technique Used to Study Exocytosis and Endocytosis

CHAYA JOSHI AND JULIO M. FERNANDEZ
Department of Physiology, University of Pennsylvania, Philadelphia, Pennsylvania 19104-6085

ABSTRACT We have studied the admittance of patch-clamped mast cells during exocytosis and found that they are adequately described by a four parameter equivalent circuit. On the basis of these measurements, we show that, contrary to current belief, when using a phase sensitive detector, small capacitance changes due to exocytosis or endocytosis should be studied by measuring current 90° out of phase, relative to the component that corresponds to changes in series resistance. We have extended the theory on phase-detectors to include the errors in the estimation of step changes of membrane capacitance. We show that the measured capacitance of a secretory granule can be up to 80% smaller than its true value, during the course of a typical mast cell degranulation. We also describe a software-based phase-detector that simplifies capacitance measurements.

INTRODUCTION

Cells transport macromolecules across their membrane by exo- or endo-cytosis. Both phenomena involve a change in membrane surface area. Since biological membranes have a constant capacitance per unit area of 1 $\mu F/cm^2$, the membrane capacitance is a useful, geometry-independent probe of surface area. Capacitance measurements can therefore be used as dynamic probes, to study membrane recycling phenomenon.

Several techniques have been developed and used to monitor capacitance changes due to the massive fusion of secretory granules with the plasma membrane (Cole, 1935; Gillespie, 1978; Jaffe et al., 1979; Peres and Bernardini, 1984). However, all these techniques lacked the resolution to detect individual granule fusion or membrane retrieval events. Using a phase sensitive detector in combination with a patch-clamp amplifier, Neher and Marty (1982) succeeded in measuring the microscopic changes in capacitance resulting from the fusion of single exocytotic vesicles. This approach has already been used to better understand exocytosis (Neher and Marty, 1982; Fernandez, Neher and Gomperts, 1984; Zimmerberg et al., 1987; Breckenridge and Almers, 1987*b*).

However, the phase detector technique has inherent errors since the probe used to study the system (i.e., the phase angle on the detector) is fixed, while the system itself is constantly changing. It is necessary to understand how these errors affect the measurements of both individual microscopic events and macroscopic capacitance changes.

Here, we have extended the theory developed on the phase detector technique to find the optimal measuring conditions and to include the errors encountered while probing membrane recycling phenomena. We have verified experimentally, on rat and mouse peritoneal mast cells, the validity of the assumptions used, and the predicted errors. Finally we have developed a simple software-based phase detector which has the advantage of not requiring any hardware other than that used for patch-clamp experiments, thereby simplifying capacitance measurements. A preliminary report of this work has appeared in abstract form (Joshi and Fernandez, 1988).

METHODS

Mast Cell Preparation and Solutions

Mast cells were obtained from adult male rats or mice by peritoneal lavage after the procedure used by Lindau and Fernandez (1986). The cells were plated on glass coverslips and incubated at 37°C in a 5% CO_2 atmosphere for at least half an hour before use. The bath solution contained 150 mM NaCl, 10 mM Hepes, 2.8 mM KOH, 1.5 mM NaOH, 1.0 mM $MgCl_2$, and 2.0 mM $CaCl_2$ (pH 7.2–7.3). The pipette solution contained 140 mM K-Glutamate, 10 mM KCl, 10 mM Hepes, 3.5 mM NaOH, 200 μM EGTA, 200 μM ATP, 7 mM $MgCl_2$, and varying concentrations of GTPγS (to induce degranulation, Fernandez et al., 1984) (pH 7.2–7.3).

Recording System

All experiments were performed using the whole-cell mode of the patch-clamp technique (Hamill et al., 1981). The command input of the patch-clamp amplifier (EPC-7, List Electronics, Darmstadt, FRG) was controlled by a PDP-11/73 computer. Data were analyzed on line and stored on disk.

Address reprint requests to Dr. J. M. Fernandez, Department of Physiology, University of Pennsylvania, Philadelphia, PA 19104-6085.

Chaya Joshi's present address is Department of Pharmacology, G-7, Mayo Clinic, Rochester, MN 55905.

Pseudo Random Binary Sequence

The Pseudo Random Binary Sequence (PRBS) technique, as described by Clausen and Fernandez (1981), was used to measure the admittance of patch-clamped mast cells. A multi-frequency voltage, $V(t)$, was applied to the membrane; the resulting current, $I(t)$, was measured, and the voltage and current were Fourier transformed to obtain the admittance $Y(\omega) = I(\omega)/V(\omega)$. The real and imaginary parts of the measured admittance were fitted by the corresponding parts of the admittance for the assumed circuit, in order to obtain the various circuit parameters (Fernandez et al., 1984). With the exception of the fast capacitance compensation, which was used to cancel the stray capacitance, no other compensation was used since the compensation circuitry would have introduced additional elements parallel with the cell, thus changing the equivalent circuit seen by the PRBS generator.

Phase Detector Experiments

Once a giga-seal was obtained, the current transients in response to voltage pulses were canceled, using the fast compensation circuitry of the patch-clamp amplifier. Upon breaking in, the new current transients were canceled using the slow capacitance and series conductance compensation circuitry. This determined the initial cell capacitance (C) and series conductance (G_s). Once compensation was complete, the membrane was subjected to a sinusoidally varying voltage (56.0 mV peak to peak, 833 Hz).

The software-based phase-detector (see Appendix) was used to monitor currents that were phase-shifted by θ–90° and θ with respect to the input voltage. θ–90° was an experimentally determined parameter which was found by making small changes in G_s (using the G_s compensation potentiometer on the patch-clamp amplifier), monitoring current at an arbitrary phase relative to the input, and varying the phase until changes in G_s were no longer accompanied by changes in current. It is important to bear in mind that the absolute value of θ (or θ–90°) is unimportant. After the phase-angle was found, C was changed (using the slow capacitance compensation circuitry on the patch clamp) by a known amount (0.1 or 1 pF), and the resulting current was monitored. This measurement served as a calibration for the capacitance.

Notice that the phase-angle θ–90 is not the same as the phase-angle ϕ used by Neher and Marty (1982). They found a phase-angle, α, by adjusting C, and varying the phase until changes in C were no longer accompanied by changes in current. Measurements of capacitance changes were then obtained at a phase-angle, ϕ, orthogonal to this α. Since the quality of the recordings depends on the choice of an appropriate phase-angle, this issue will be addressed further in the results and discussions.

RESULTS

Equivalent Circuit for a Mast Cell

A mast cell membrane may be modeled as shown in Fig. 1 *a*, by a resistor (conductance G) in parallel with a capacitor C. Upon patch-clamping the cell, the pipette introduces a stray capacitance C_p, while the tip introduces an additional resistance (conductance G_s) in series with the cell membrane.

A straightforward way to test the validity of the model is to use the PRBS technique (Clausen and Fernandez, 1981) to measure the admittance, $Y(\omega)$, of the cell. Values for R_s ($=1/G_s$), C, and G can be derived by curve fitting this measured admittance with the admittance predicted by the model circuit (see the next section). A comparison of the measured admittance and the fitted admittance (the admittance obtained using the derived parameters) should be a good indication of the validity of the assumed equivalent circuit.

We performed such measurements on a mast cell before, during, and after complete degranulation. Curve-fitting of the real and imaginary components of the measured admittance (see Eq. 1b below) gave (for the experiment shown in Fig. 1 *b*) R_s = 3.8 MΩ and C = 11 pF before stimulation; R_s = 4.0 MΩ and C = 36 pF after degranulation. C_p was a constant 1.2 pF while G was <1 nS throughout the experiment. Fig. 1 *b* shows the two components of $Y(\omega)$ before (upper traces) and after (lower traces) degranulation. The components of the fitted admittance (thin line) are indistinguishable from the corresponding components of the measured admittance (heavy line) except at high frequencies. Since the fitted curves were in excellent agreement with the experimentally measured curves, we

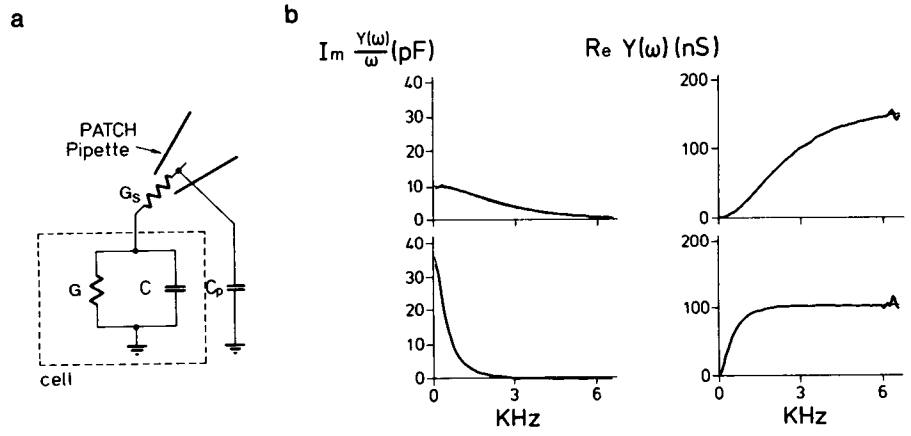

FIGURE 1 (*a*) Equivalent circuit for a patch-clamped mast cell. (*b*) Experimental confirmation of the equivalent circuit for a patch-clamped rat mast cell. Resistive (Re ($Y[\omega]$) and capacitive (Im($Y[\omega]/\omega$) components of the admittance before (*top*) and after (*bottom*) degranulation. Measured admittance (*heavy line*) is well described by equation 1b as shown by the fits (*thin line*). Cells were stimulated by intracellular perfusion with 50 μM GTPγS.

concluded that the circuit of Fig 1 *a* was a valid approximation for a patch-clamped mast cell before, during (not shown), and after degranulation.

Fig. 2 *a* shows the time course of the two components of the measured admittance during a degranulation. As expected, the capacitance, which is the low frequency asymptote of $Im(Y[\omega]/\omega)$ (Eq. 1b, below), increases as the cell degranulates. By curve fitting the admittance as it evolves in time, it is possible to reconstruct the time course of the various circuit parameters. Thus one can obtain an estimate for the ranges over which the various parameters vary during a degranulation in which all the secretory granules contained in the cell fuse with the plasma membrane. The results of such an experiment are shown in Fig. 2 *b*. As shown in the figure, upon stimulation, the membrane capacitance increases smoothly by about a factor of 4, while both the membrane conductance and the series conductance fluctuate rapidly through the experiment. It is safe to conclude that changes in conductance (both membrane and series) are unrelated to changes in capacitance. The PRBS technique has the advantage that it allows for the reconstruction of C, G, and G_s through a degranulation. However, as mentioned earlier, it lacks the resolution necessary to monitor individual fusion events. The phase detector technique, in contrast, is capable of resolving small changes in capacitance.

Phase Detector Theory

We will begin our analysis of the phase-detector technique following Neher and Marty (1982). The admittance $Y(\omega)$ ($\omega = 2\pi f$) for the circuit in Fig. 1 *a* is given by

$$Y(\omega) = \frac{G + j\omega c}{1 + G/G_s + j\omega c/G_s} + j\omega C_p \qquad (1a)$$

or, in terms of the real and imaginary components as

$$Y(\omega) = \frac{G(1 + G/G_s) + \omega^2 C^2/G_s}{(1 + G/G_s)^2 + (\omega C/G_s)^2} + j\omega\left[C_p + \frac{C}{(1 + G/G_s)^2 + (\omega C/G_s)^2}\right]. \qquad (1b)$$

From basic circuit theory, when a sinusoidally varying voltage, V, is applied across the circuit of Fig. 1 *a*, a sinusoidally varying current, I, results. I has the same frequency as V, but is phase-shifted (phase = arg[Y]) relative to V. Furthermore, since $I = VY$, changes in current amplitude reflect changes in admittance which in turn reflect changes in the circuit parameters C, G, or G_s. When these changes are small, the corresponding changes in current may be calculated by linearizing the system as follows

$$\Delta I_G = V\frac{\partial Y}{\partial G}\Delta G = VB^2\Delta G \qquad (2a)$$

$$\Delta I_c = V\frac{\partial Y}{\partial C}\Delta C = j\omega VB^2\Delta C \qquad (2b)$$

$$\Delta I_{G_s} = V\frac{\partial Y}{\partial G_s}\Delta G_s = (G/G_s + j\omega C/G_s)^2 VB^2\Delta G_s, \qquad (2c)$$

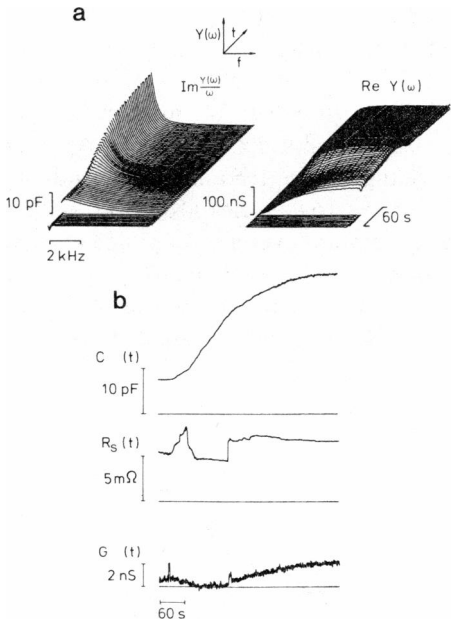

FIGURE 2 (*a*) Evolution of the components of the admittance of a rat mast cell, while degranulating. (*b*) Time course of capacitance and conductance(s) during degranulation in a mast cell measured by the PRBS technique. The cells were stimulated as in Fig. 1 *b*.

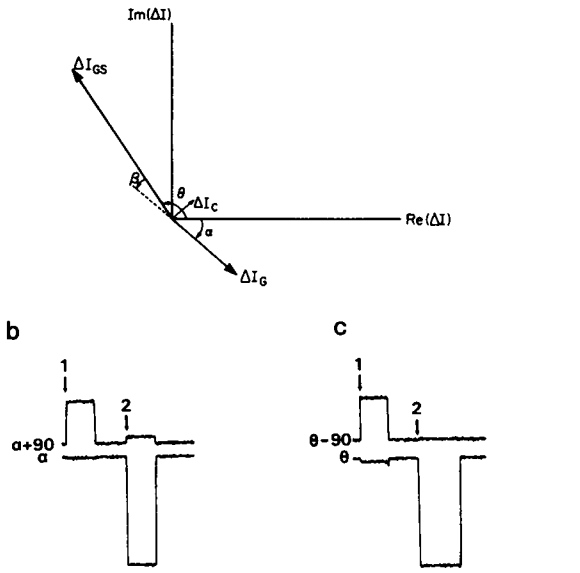

FIGURE 3 (*a*) Complex-space representation of the phasors ΔI_G, ΔI_C, and ΔI_{G_s} which represent changes in current due to small changes in G, C, and G_s respectively (see Eqs. 2a, b, and c). The total change in current, ΔI is the sum of the three phasors. (*b* and *c*) Making a choice between $\alpha/\alpha + 90°$ (*b*, *bottom/top*) or θ/θ–90 (*c*, *bottom/top*). The traces show the component of current at each of the phase angles. Arrow 1 represents a 100 fF capacitance change while arrow 2 represents a 10 nS change in series conductance.

where

$$B^2 = (1 + G/G_s + j\omega C/G_s)^{-2} \quad (3a)$$

$$\alpha = \arg(\Delta \mathbf{I}_G) = -2\tan^{-1}\left(\frac{\omega C}{G + G_s}\right) \quad (3b)$$

$$\theta = \arg(\Delta \mathbf{I}_{G_s}) = 2\left[\tan^{-1}\left(\frac{\omega C}{G}\right) - \tan^{-1}\left(\frac{\omega C}{G + G_s}\right)\right] \quad (3c)$$

$$\beta \equiv 180° + \alpha - \theta = 180° - 2\tan^{-1}\left(\frac{\omega C}{G}\right) \quad (3d)$$

The total change in current, $\Delta \mathbf{I}$ is the sum of $\Delta \mathbf{I}_G$, $\Delta \mathbf{I}_{G_s}$, $\Delta \mathbf{I}_C$. Fig. 3 *a* is a complex-space (or phasor) representation of the three components of $\Delta \mathbf{I}$. From Eq. 2, it can be seen that $\Delta \mathbf{I}_G$ is 90° out of phase with respect to $\Delta \mathbf{I}_C$, and is almost antiparallel to $\Delta \mathbf{I}_{G_s}$. On the phasor-diagram of Fig. 3 *a*, the real component of $\Delta \mathbf{I}$ reflects changes in current that are in-phase with the applied voltage while the imaginary component measures changes that are 90° out-of-phase with respect to the input. Using a two-channel phase detector (see Appendix), the amplitude of the current can be measured at arbitrary phase angles, ϕ and $\phi \pm 90°$ relative to the input.

Suppose that during an experiment, the capacitance, membrane conductance, and series conductance changed by ΔC, ΔG, and ΔG_s respectively. A phase detector monitoring current that is phase-shifted by $\alpha + 90°$ with respect to the input would then measure a change in current, $\Delta \mathbf{I}_{\alpha+90°}$, of magnitude

$$|\Delta \mathbf{I}_{\alpha+90°}| = V|B^2|\omega\left(\Delta C + \frac{2GC}{G_s^2}\Delta G_s\right) \quad (4a)$$

while a detector monitoring current phase-shifted by θ–90° would measure a change in current, $\Delta I_{\theta-90°}$, which, to first order in $(G/\omega C)$ is of magnitude

$$|\Delta \mathbf{I}_{\theta-90°}| = V|B^2|\left(\omega\Delta C + \frac{2G}{\omega C}\Delta G\right) \quad (4b)$$

Choosing the Correct Phase Angle

Before proceeding any further, it is therefore important to decide whether the phase-angle $\theta - 90°$ or $\alpha + 90°$ is more appropriate to monitor changes in capacitance for mast cells. We simulated a mast cell with an RC network (G = 1 nS, C = 5.6 pF, G_s = 80 nS) connected to the input of the patch-clamp amplifier. For this cell, $\alpha = -38.6°$, θ = 137.3°, and β = 4.1° (Eq. 3). α was found experimentally by making small changes in C (ΔC = 100 fF) and adjusting the phase angle until the current was no longer affected by changes in C. Fig. 3 *b*, arrow 1 shows a 100 fF capacitance step and its effects on the current at $\alpha + 90°$ (top trace) and at α (bottom trace; there is no effect due to the choice of α). The effects of small changes in G_s (ΔG_s = 10 nS, Fig. 3 *b*, arrow 2) on the currents at both α (bottom) and $\alpha + 90°$ (top) was monitored. As shown in the figure, even a small change in G_s makes a sizable contribution (~15% for this experiment) to $\Delta \mathbf{I}_{\alpha+90°}$. This phase angle is therefore sensitive to changes in G_s. This calibration procedure was then repeated except that this time the phase angle, θ–90°, was found by making small changes in G_s (ΔG_s = 10 nS) and minimizing the effect on the measured current (Fig. 3 *c*, arrow 2, the top trace is unaffected). C was then changed by 100 fF (Fig. 3 *c*, arrow 1), and $\Delta \mathbf{I}_\theta$ (bottom trace), and $\Delta \mathbf{I}_{\theta-90°}$ (bottom trace) were measured. Since we are mainly interested in capacitance changes (i.e., changes in $\Delta \mathbf{I}_{\theta-90°}$), the projection of the change in capacitance on $\Delta \mathbf{I}_\theta$ can be ignored. In mast cells the predominant changes are in G_s and not in G (see Fig. 2 *b*), therefore, it is more appropriate to monitor capacitance changes by measuring the current phase-shifted by θ–90°. In all that follows, we will be concerned with the phase angles θ and θ–90° alone, unless explicitly stated otherwise. Changes in the amplitude of current phase-shifted by θ–90° are referred to as capacitance changes, while changes at a phase θ are referred to as conductance changes.

Measuring Individual Fusion Events

Fig. 4 shows a recording of $\Delta \mathbf{I}_{\theta-90°}$ from a degranulating mast cell. The figure illustrates the step increases in capacitance which are thought to correspond to the fusion of individual secretory granules as the mast cell degranulates (Fernandez et al., 1984). Since the detector remains fixed while the cell degranulates, how far in this capacitance staircase can the size of an individual granule be reliably measured?

In the course of an experiment both $|B^2|$ and θ change (Eq. 3 *a* and *c*), due to changes in membrane properties (conductance or capacitance) and seal characteristics. Figs. 5 *a* and *b* show $|B^2|$ and θ at three different input frequencies as a function of membrane capacitance, assuming a series resistance of 10 MΩ. As shown in the figure, the changes in both θ and $|B^2|$ depend on the input frequency. At low frequencies (100 Hz), both θ and $|B^2|$ remain fairly constant over a large range of capacitances. As the frequency increases, θ and $|B^2|$ change much more for equivalent changes in capacitance. At very high frequencies (10 KHz; not shown), although θ is close to 0° and

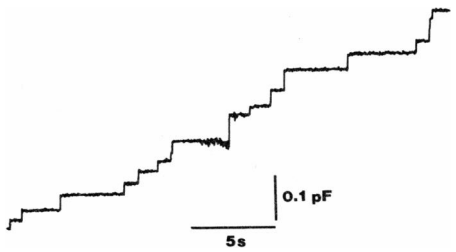

FIGURE 4 Capacitance steps observed in a mouse peritoneal mast cell using the software phase-detector at θ–90°. Notice the absence of drifts.

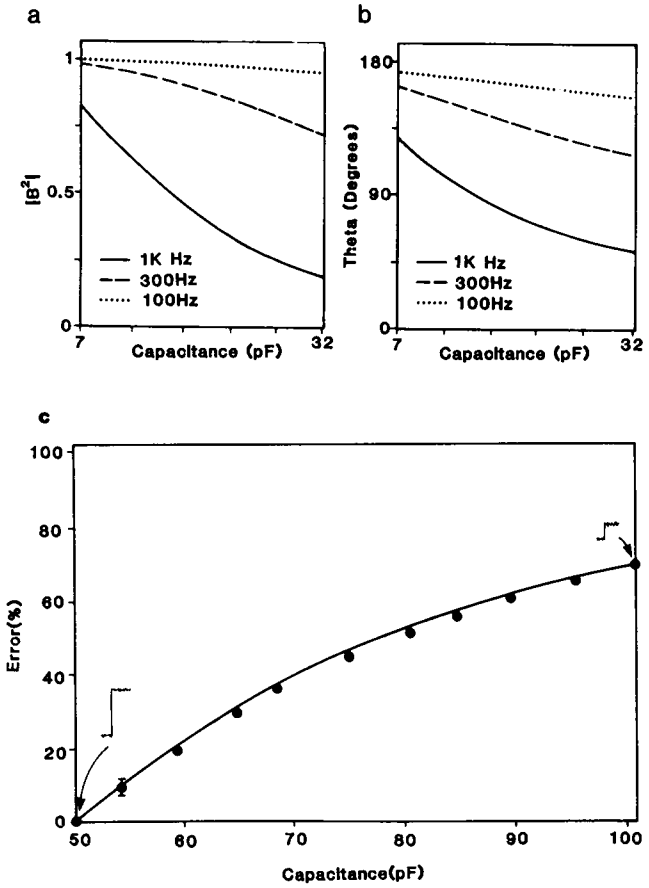

FIGURE 5 $|B^2|$ (Eq. 3a, Fig. 5 *a*), and phase angle θ (Eq. 3b, Fig. 5 *b*), as a function of capacitance at various stimulus frequencies. (*c*) Verification of Eq. 5. Comparison of experiment (*filled circles*) with theoretical prediction (*solid curve*). The insets show the size of a 1 pF step at 50 pF (*left*) and at 100 pF (*right*).

remains constant as the capacitance increases, $|B^2|$ is very sensitive to changes in capacitance or conductance.

Since θ and $|B^2|$ are changing during an experiment, the phasor $\Delta\mathbf{I}_C$ also changes. The detector on the other hand, remains fixed. Initially (subscript i), a detector at θ–90° measures a 100 fF step change in capacitance as a change n current of magnitude $\Delta I'_{Ci} = 100\ \mathrm{V}|B_i^2|\omega \cos(\beta_i)$ fA. At the same time, the detector at θ would measure a change in current $\Delta I''_{C_i} = 100\ \mathrm{V}|B_i^2|\omega \sin(\beta_i)$ fA (this change is usually negligible). In the course of the experiment, due to changes in C, G_s, G, the vector $\Delta\mathbf{I}_C$ representing a 100 fF change has moved both in amplitude and in phase. Its new amplitude (subscript f), is $\Delta I_{C_f} = 100\ \mathrm{V}|B_f^2|\omega$. The detector at θ–90° therefore measures the same 100 fF step as a current of magnitude $100\ \mathrm{V}|B_f^2|\omega \cos[\beta_i + (\alpha_f - \alpha_i)]$. The percent error, E, in the measurement of the step amplitude is therefore

$$E = 100 * \left\{1 - \frac{|B_f^2|}{|B_i^2|} \frac{\cos[\beta_i + (\alpha_f - \alpha_i)]}{\cos \beta_i}\right\} \qquad (5)$$

Furthermore, the 100 fF change in capacitance will now manifest itself as a $100\ \mathrm{V}|B_f^2|\omega \sin[\beta_i + (\alpha_f - \alpha_i)]$ change in the current that is phase-shifted by θ. This term may be detectable so there is an additional conductance change that accompanies the capacitance change. A similar analysis holds for conductance changes (i.e., due to changes in circuit parameters, the vector $\Delta\mathbf{I}(G, G_s)$ is moving, while the detector is fixed). As a result, conductance changes may manifest themselves as capacitance changes.

Verification of the Error Equation

The error equation (Eq. 5), predicts that the size of a capacitance step changes artifactually during an experiment. This hypothesis was tested by connecting a large model cell (a 50 pF capacitor in series with a 4 MΩ resistor) to the input of the patch-clamp amplifier. After cancelling the current transients, the phase angle θ–90° was found. Neither θ–90° (i.e., the detector), nor G_s were changed during the experiment. Using the compensation circuitry, the capacitance was increased in 5 pF increments and the size of a 1 pF capacitance step (i.e., $\Delta C = 1$ pF) was measured at each value of C. The % error was calculated as 100 (1 − size at C/size at $C_i = 50$ pF). Fig. 5 *c* shows the results of such an experiment (filled circles) along with the curve corresponding to the theoretical predictions of Eq. 5. The experimental results agree with the theory within measuring error (a representative error bar has been shown for one data point). The insets of Fig. 5 *c* show the change in current due to a 1 pF capacitance step at 50 pF (left) and the same step measured at 100 pF (right).

DISCUSSION

Choosing the Right Phase Angle

In all our experiments, the current response phase-shifted by some phase-angle, ϕ, relative to the stimulus voltage, is measured. Changes in current will be proportional to changes in capacitance if ϕ is chosen correctly. Experimentally (Fig. 3 *b* and *c*), we had determined that θ–90° was the appropriate phase angle for mast cells. In this section we will attempt to explain the experimental findings quantitatively.

Since β, the difference between $\theta - 90°$ and $\alpha + 90°$ (Eq. 3 *d*) is typically small, for small changes in C, G_s, and G, $\Delta I_{\alpha+90°} \simeq \Delta I_{\theta-90°}$. Therefore the current measured at both phase angles is proportional to changes in C (Neher and Marty, 1982). What happens when β is measurable? Consider a cell like the one from Fig. 2 *b* for which $C = 8$ pF, $G_s = 100$ nS, and $G = 1$ nS. For this cell, $\beta \simeq 3°$. What happens now if C, G_s, and G change by 100 fF, 20 nS, and 0.2 nS respectively? From Eq. 4 *a*, the change in G_s contributes ~¼th of the total change in the current measured at $\alpha + 90°$ $\{[2GC/G_s^2]\ (\Delta G_s/\Delta C) \sim 0.3\}$. The change in G on the other hand contributes only 2% of the total change in current at θ–90° $\{[2G/\omega^2 C](\Delta G/\Delta C) \sim 0.02\}$. Due to the choice of θ–90°, the change in G_s makes

no contribution at all to this current. We therefore conclude that for good cells (small G, small β), both phase angles are equivalent. However, by making measurement at θ–90°, one can make good measurements even on those cells for which G is higher (β is larger).

Reducing the Errors

As shown in Fig. 5 *a* and *b*, since the circuit parameters are constantly changing during an experiment, the phase-angle and $|B^2|$ are also constantly changing; as a result, the size of a capacitance step changes artifactually (insets of Fig. 5 *c*). In this section we discuss the effects of circuit parameters on the errors, E (%).

The series resistance can affect the reliability of the phase detector. Depending on the initial series resistance, and assuming that it remains constant through an experiment, the errors may increase at different rates during an experiment. Fig. 6 *a* is a plot of the errors at different series resistances. The series resistances chosen represent very good (5 MΩ), normal (10 MΩ), and poor access (20 MΩ).

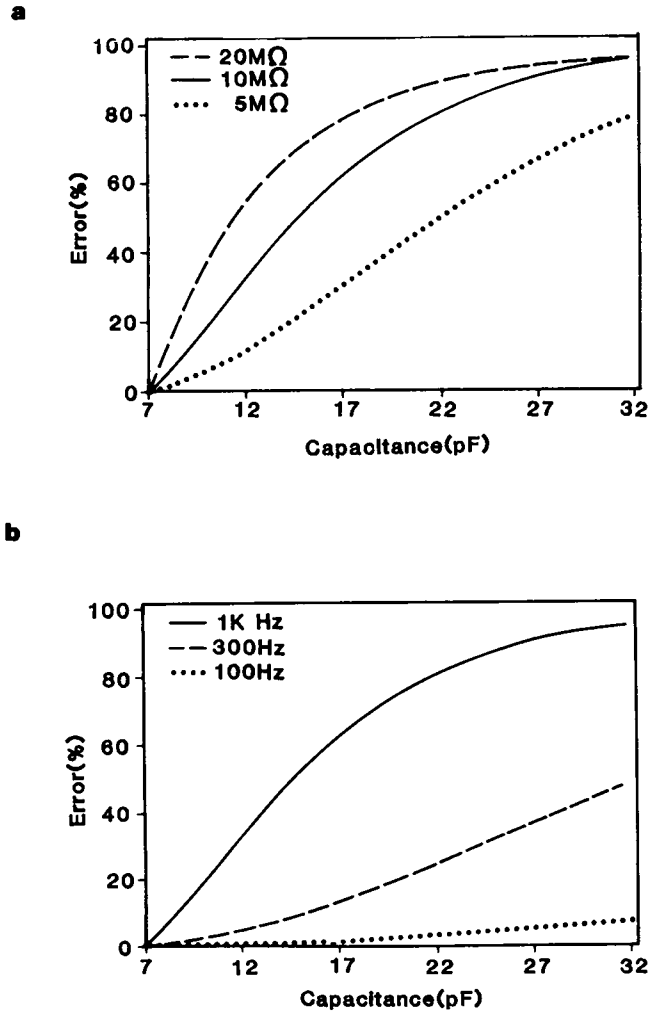

FIGURE 6 Prediction of errors (Eq. 5) as a function of capacitance for an exocytotic process at (*a*) different access resistances (f = 1 KHz, G = 10 pS) and (*b*) different frequencies (G_s = 100 nS, G = 10 pS).

The input frequency is also an important variable in these experiments. In Fig. 6 *b* we have plotted E as a function of C, for an exocytotic process, at three different frequencies. The capacitance range chosen is typical of a complete degranulation in adult rat mast cells. At low frequencies (e.g., 100 Hz), the attenuation of a 100 fF step is <10% through a degranulation, while at higher frequencies (e.g., 1,000 Hz), by the time the capacitance has increased by 3 pF, the measured size of a capacitance step is 20% of its true value.

Based on these results, it appears that a low frequency stimulus sinewave is ideal to perform experiments since the phase-angle θ remains constant; hence the errors are low throughout the experiment. However, the magnitude of ΔI_C for a fixed ΔC is proportional to ω. As a result, at low ω, the signal to noise ratio decreases and step changes in capacitance due to single fusion/retrieval events cannot be resolved. Furthermore, when ω is so low that the capacitive impedance and the membrane resistance are comparable, even small changes in membrane conductance can make a sizeable contribution to the current that is phase-shifted by θ–90°. ω should therefore be chosen such that $G \ll \omega C \ll G_{s,min}$ throughout the experiment.

Effect of Errors on Amplitude Histograms

Amplitude histograms have been constructed using steps such as those shown in Fig. 4 to study the size distribution of secretory granules (Neher and Marty, 1982; Fernandez et al., 1984; Breckenridge and Almers, 1987*a*). Since capacitance steps are artifactually attenuated as the capacitance increases, a histogram constructed from steps in the initial phases of a degranulation is representative of the true granule surface area histogram. In contrast, a histogram constructed using steps from later stages in the degranulation will be skewed to the left (more small steps measured). For endocytotic processes, histograms tend to be skewed to the right. Due to the correlation of the steps with single organelles, it is very important to be able to measure these steps reliably.

The definition of a reliable range for the detector depends on the system and the magnitude of capacitance changes being studied. It is possible to correct some of the errors provided (*a*) one has records of both ΔI_θ, and $\Delta I_{\theta\text{-}90°}$, (*b*) the initial values of C and G_s are known, and (*c*) the capacitance steps being studied are large (~100 fF). The last stipulation is necessary since under those circumstances, ΔI_C has a measurable contribution to ΔI_θ as soon as the detector (at θ–90°) and ΔI_C get out of phase with respect to each other. As a result, the ratio of ΔI_θ and $\Delta I_{\theta\text{-}90°}$ may be used to compute the change in α. Thus α_f and $|B_f^2|$ can be calculated. Hence the true size of the step may be determined.

APPENDIX

A Software Based Phase-Detector

For our purposes, a two-channel phase-sensitive detector is a device that measures those components of membrane current that are phase shifted by arbitrary amounts, P and $P \pm 90°$, with respect to the stimulus voltage. For a complete description of the theory on phase-sensitive detectors, see Horowitz and Hill (1983). What follows is a brief description of an algorithm to implement a simple software based two-channel phase-sensitive detector such as the one used in this paper.

Fig. 7 illustrates a flow chart for the computer programming of the phase detector algorithm. Upon startup (Box 1), we generate three waveforms: $W(j)$ which is a high-resolution sinewave (400 points per cycle, or 0.9°; the resolution can be improved if desired by increasing the range on j); $D^0(k)$ and $D^{90}(k)$ which are low resolution (4 points per cycle) sinewaves, phase-shifted by 0^0 and 90^0 relative to $W(j)$. The index k runs from 1 to NP (= 4 * number of cycles over which integration is performed, see below) while j ranges between 1 and 400 NP.

Boxes 2 and 3 make up a device that constructs the stimulus waveform $S(k)$ from $W(j)$. $W(j)$ has 100 times the resolution required for $S(k)$. Therefore, to construct $S(k)$, we have to select every hundredth point from $W(j)$. If $S(0) = W(0)$, then the stimulus $S(k)$ will be in-phase with $D^0(k)$. On the other hand, if $S(0) = W(100)$, then $S(k)$ will be in-phase with $D^{90}(k)$ and 90^0 out-of-phase with respect to $D^0(k)$. Therefore, by defining $S(0) = W(P)$, where P ranges from 0 to 200, it is possible to phase-shift S by arbitrary amounts P and $P \pm 90^0$ relative to the detectors $D^0(k)$ and $D^{90}(k)$ respectively.

Box 4 stimulates the cell and samples the response $R(k)$. Since $S(k)$ is defined by four points per cycle, it must be low-pass filtered (to generate a smoothly varying sinusoid) before stimulating the cell.

Finally, Box 5 performs the actual phase-detector function. The zero-frequency component of the product $R(k)$ $D^j(k)$ ($j = 0$ or 90) is sensitive to the phase difference between $D^j(k)$ and $R(k)$. This zero-frequency component can be extracted by integrating the product over one cycle. To improve the signal-to-noise ratio, we have chosen to integrate it over several (usually 8 to 10) cycles. Based on earlier discussions (see Methods), the capacitance sensitive current, C, is phase-shifted by $-P + 90^0$ relative to the input while the conductance sensitive current, G, is phase-shifted by $-P$ relative to the input (where P corresponds to $-\theta$ of the Methods section). The actual definitions of C and G are given in Box 5.

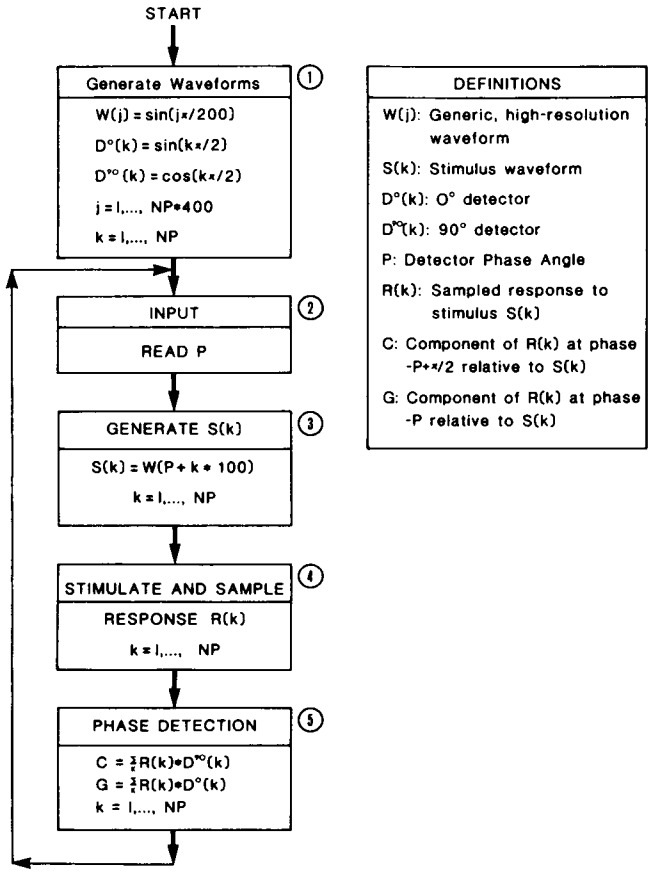

FIGURE 7 Flow-chart for a software-based phase-detector.

We are grateful to Dr. G. Alvarez de Toledo for experiments, discussions, and for providing Fig. 4. The authors are also grateful to Drs. D. E. Clapham and Y. E. Goldman for valuable suggestions on the manuscript. The experiments of Figs. 1 and 2 were done at the Department of Membrane Biophysics, MPI, Goettingen, West Germany.

This paper was supported by National Institutes of Health grant GM-38857-01.

Received for publication 24 August 1987 and in final form 4 February 1988.

REFERENCES

Breckenridge, L. J. and W. Almers. 1987*a*. Final steps in exocytosis observed in a cell with giant secretory granules. *Proc. Natl. Acad. Sci. USA.* 84:1945–49.

Breckenridge, L. J., and W. Almers. 1987*b*. Currents through the fusion pore that forms during exocytosis. *Nature (Lond.).* 328:814–817.

Clausen, C., and J. M. Fernandez. 1981. A low cost method for rapid transfer function measurement with direct application to biological impedance analysis. *Pfluegers Arch. Eur. J. Physiol.* 390:290–295.

Cole, K. S. 1935. Electric impedance of hipponoe eggs. *J. Gen. Physiol.* 18:877–887.

Fernandez, J. M., E. Neher, and B. D. Gomperts. 1984. Capacitance measurements reveal stepwise fusion events in degranulating mast cells. *Nature (Lond.).* 312:453–455.

Gillespie, J. I. 1979. The effect of repetitive stimulation on the passive electrical properties of the presynaptic terminal of the squid giant synapse. *Proc. R. Soc. Lond. B. Biol. Sci.* 206:293–306.

Hamill, O. P., A. Marty, E. Neher, B. Sakmann, and F. J. Sigworth. 1981. Improved patch-clamp techniques for high-resolution current recording from cells and cell-free membrane patches. *Pfluegers Arch. Eur. J. Physiol.* 391:85–100.

Horowitz, P., and W. Hill. 1983. The Art of Electronics. Cambridge Univ. Press, New York.

Jaffe, L. A., S. Hagiwara, and R. T. Kado. 1978. The time course of cortical vesicle fusion in sea urchin eggs observed as membrane capacitance changes. *Dev. Biol.* 67:243–248.

Joshi, C., and J. M. Fernandez. 1988. An analysis of the phase-detector technique to study exocytosis. *Biophys. J.* 53:362. (Abstr.)

Lindau, M., and J. M. Fernandez. 1986. A patch-clamp study of histamine secreting cells. *J. Gen. Physiol.* 88:349–368.

Neher, E., and A. Marty. 1982. Discrete changes of cell membrane capacitance observed under conditions of enhanced secretion in bovine adrenal chromaffin cells. *Proc. Natl. Acad. Sci. USA.* 79:6712–6716.

Peres, A., and G. Bernardini. 1985. The effective membrane capacity of Xenopus eggs: its relation with membrane conductance and cortical granule exocytosis. *Pfluegers Arch. Eur. J. Physiol.* 404:266–272.

Zimmerberg, J., M. Curran, F. S. Cohen, and M. Brodwick. 1987. Simultaneous electrical and optical measurements show that membrane fusion precedes secretory granule swelling during exocytosis of beige mouse mast cells. *Proc. Natl. Acad. Sci. USA.* 84:1585–89.